Channel Modeling of MI Underwater Communication using Tri-directional Coil Antenna

Hongzhi Guo and Zhi Sun
Department of Electrical Engineering
State University of New York at Buffalo, Buffalo, NY 14260
E-mail: {hongzhig, zhisun}@buffalo.edu.

Pu Wang
Department of Electrical Engineering & Computer Science
Wichita State University, Wichita, Kansas 67260
E-mail: pu.wang@wichita.edu

***Abstract*—While underwater wireless communications have been investigated and implemented for decades, existing solutions still have difficulties in establishing reliable and low-delay wireless underwater links among small-size devices. The Magnetic Induction (MI) communication technique is among the promising solutions due to its advantages in low propagation delay and less susceptibility to the transmission environments. To date, existing MI models cannot accurately characterize the complex underwater MI channels, especially in the shallow water with omnidirectional antennas. In this paper, an analytical channel model is developed for underwater MI communication system with Tri-directional coil (TD coil), which is derived based on the rigorous electromagnetic field analysis. The MIMO channel between the tri-directional coil antennas are characterized under the complex influences from the water absorption as well as the surface reflection and lateral waves. To validate the channel model, we compare the theoretical results with simulations derived by the COMSOL Multiphysics simulation tool.**

I. Introduction

Underwater wireless communication enables the real-time information sharing among networks of various underwater devices, such as underwater sensors and unmanned vehicles/robots [1]. Although the underwater wireless solutions have been investigated and implemented for decades long, existing techniques that are based on acoustic wave, optical wave, or electromagnetic (EM) wave still have difficulties in establishing reliable and low-latency wireless underwater links among small-size devices.

Recently, the Magnetic Induction (MI) techniques have shown great potentials in wireless communications in RF-challenging environments, including underground [2] and underwater [3]. Due to the unique advantages in low propagation delay and less susceptibility to the transmission environments [4], MI techniques become a promising solution to address the aforementioned challenges in underwater wireless communications. First, MI relies on the near field component of the magnetic field generated by coil antennas [2], which penetrates the lossy underwater medium much more efficiently than the far field EM waves. Second, the MI signals propagate at the speed of light, much faster than the acoustic waves. Hence, the propagation delay in MI is extremely small. Third, the impacts of multipath fading and scattering are minimized in the near field-based MI communications. As a result, the MI underwater channel is reliable and predictable.

The MI underwater channel model is essential to design and implement the underwater communication system as well as the whole networking protocol stack. In [4] and [5], the MI channel models are developed for MI systems with fixed coil antennas in homogeneous water environments. However, those existing MI underwater models still cannot fully characterize the complex underwater MI channels, especially in the shallow water and with highly dynamic antenna orientations. In particular, first, the impacts of lossy underwater medium due to the water conductivity has not been thoroughly modeled. In [5], the material absorption in conductive sea water is not characterized. In [4], although the additional path loss due to material absorption is considered, the impact of lossy medium on the MI mutual coupling is neglected. In fact, the coil's resistance can be greatly increased in lossy medium since the magnetic flux in vicinity of the coil is no longer real. Second, the effects of water surface in the shallow water region on the MI communications have not been modeled. In [5], [4], the considered underwater environment is infinite where no boundary exists. In fact, near the surface of water, the lateral wave is dominant, which could enable long distance underwater communication [6]. Hence, the existing underwater MI channel models actually underestimate MI's performance.

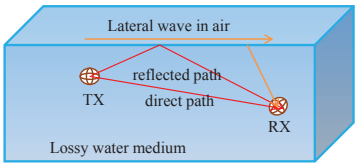

Fig. 1. Illustration of MI communication using Tri-directional coil (TD coil) antenna in underwater environment.

In this paper, an accurate and comprehensive underwater channel model is developed for MI communication systems, which can characterize the signal propagation in all types of underwater environments including shallow water. Moreover, the impact of the dynamic antenna orientation is investigated. To mitigate such impact, an effective solution, i.e., the MI transceivers with Tri-directional coil (TD coil), is proposed and characterized in the developed MI underwater channel model. The TD coil consists of three mutually perpendicular unidirectional (UD) single coils. Each one of the three UD coils forms a beam along one of the three axes in the Cartesian coordinate. The considered wireless channel and the MI system are illustrated in Fig. 1. To derive the channel model in this paper, the EM fields generated by coils with arbitrary orientation is first investigated by utilizing the rotation theorem [7] for vector spherical wave functions, which yields a rigorous and succinct formulation of the radiation pattern of the TD coil. Then, the MI signal propagation in the complicated underwater environment is analyzed. The effect of the water surface is modeled by investigating the magnetic field from the direct path, reflected path, and lateral waves. Next, the additional resistance of the MI transceivers caused by the lossy underwater medium is quantitatively analyzed and validated

† This work was supported by the US National Science Foundation (NSF) under Grant No. CNS-1446484.

by Finite Element Method (FEM) simulations. After that, an equivalent circuit model is presented and the frequency-dependent channel path loss, bandwidth, and capacity are obtained. Finally, through numerical evaluation, the channel characteristics of MI-based underwater channel are discussed.

The rest of the paper is organized as follows. Section II first presents the radiation model for TD coil with arbitrary orientations. Then the magnetic field intensity in any underwater environment is analyzed by introducing the lateral waves. Based on the field analysis, Section III investigates the self-inductance and mutual inductance of the underwater MI system. The important channel parameters, including the path loss, bandwidth, and capacity, are derived. The numerical results are discussed in Section IV. Finally, we conclude this paper in Section V.

II. Underwater Field Analysis for MI System with Tri-directional Coils

In this section, the EM field of the arbitrarily orientated TD coil is first investigated. Then, the radiated fields by the TD coil and the lateral wave caused by the water surface are formulated. Last, the developed field model is verified by the FEM simulation using Comsol Multiphysics. In the rest of this paper, we use boldface lowercase letters for vectors and boldface capital letters for matrices. For a vector $\mathbf{h}_r$, h_r denotes its magnitude and $\hat{r}$ denotes its direction. For a matrix $\mathbf{I}$, $\mathbf{I}^T$ denotes its transpose and $\mathbf{I}^{-1}$ denotes its inverse. For a complex number x, $\Re x$ denotes its real part.

A. Arbitrarily Orientated Tri-directional Coil

Referring to Fig. 1, since the underwater environment is highly dynamic, it is impractical to fix the position and orientation of the antenna. Hence, we consider both the transmitting TD coil and the receiving TD coil are arbitrarily orientated. Also, each UD coil is assumed to be an independent infinitesimal magnetic dipole.

For an arbitrarily orientated TD coil in Fig. 2(a), the current I_0, radius a, and number of turns N are the same for the three UD coils C_1, C_2 and C_3. The default system parameters include: coil antenna radius is 5 cm; number of turns for each coil is 10; and the operating frequency is 10 MHz. Since the coil radius is much smaller than wavelength, the phase shift among the three UD coils can be ignored. The dipole moment for each UD coil is $\mathbf{m}_l = m \cdot \mathbf{n}_l$, where $l = 1, 2, 3$, $m = \pi a^2 N I_0$, and $\mathbf{n}_l = [n_{lx}, n_{ly}, n_{lz}]$. We use a unit vector $\mathbf{n}_l$ to denote coil l's orientation which is perpendicular to its plane.

Next, the dipole moment is decomposed into $[m \cdot n_{lx}, m \cdot n_{ly}, m \cdot n_{lz}]$. Then, we can add together the three dipole moments on the same direction. For instance, the dipole moment along x-axis can be written as $\mathbf{m}_x = [m \cdot (n_{1x} + n_{2x} + n_{3x}), 0, 0]$.

By using the same procedure, we can obtain $\mathbf{m_y}$, and $\mathbf{m_z}$. Consider the dipole moments $\mathbf{m_x}$, $\mathbf{m_y}$, and $\mathbf{m_z}$ relating to three equivalent UD coils which are perpendicular to each other, we formally substitute an arbitrarily orientated TD coil with a TD coil whose three axes are the same as the Cartesian coordination's axes as shown in Fig. 2(d).

In the following analysis, the UD coils with axis x, y, and z in Fig. 2(d) are denoted by C_x, C_y and C_z, respectively. The equivalent current in the corresponding coil is denoted by I_x, I_y and I_z, respectively.

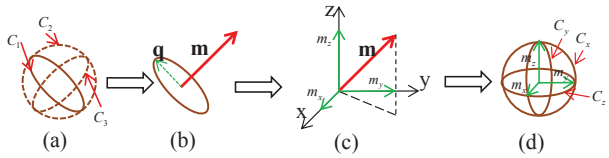

Fig. 2. Decomposition of magnetic dipole moment and equivalent TD coil.

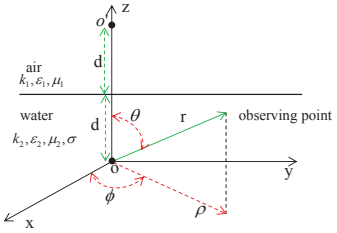

Fig. 3. System coordination. The transmitting TD coil is located at the origin o.

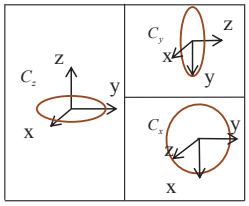

Fig. 4. Coordination for each UD coil where (1) can be applied.

B. Radiated Fields by Tri-directional Coil

Before embarking on the analysis, the system coordination is first shown in Fig. 3. The transmitter is located at the origin o and the radial distance is denoted by ρ, which will be utilized to derive the lateral wave. Also, the air-water interface is located at $z = d$. The wavenumber, permeability, and permittivity are denoted by k, μ and ϵ, respectively. As shown in the figure, we use subscript 1 and 2 to denote the corresponding environmental parameters in air and water, respectively.

The well-known radiated magnetic fields from a UD coil are [8],

$$\begin{cases} \mathbf{h}_r &= \frac{jka^2 N I_z \cos\theta}{2r^2}\left[1+\frac{1}{jkr}\right]e^{-jkr}\hat{r}, \\ \mathbf{h}_\theta &= \frac{-k^2 a^2 N I_z \sin\theta}{4r}\left[1+\frac{1}{jkr}-\frac{1}{(kr)^2}\right]e^{-jkr}\hat{\theta}, \\ \mathbf{h}_\phi &= 0, \end{cases} \tag{1}$$

where $j = \sqrt{-1}$, $k = \omega\sqrt{\mu\epsilon}$, ω is the angular frequency, and r is the distance from origin. For lossy water medium, $\epsilon = \epsilon_2 - j\frac{\sigma}{\omega}$, where σ is the conductivity.

It should be emphasized that the above formulas are derived in a spherical coordination where z axis is the same as the coil's axis and the origin is the center of the coil. Therefore, in order to find the radiated fields from a TD coil, (1) has to be calculated three times in the corresponding coordination for each UD coil as shown in Fig. 4. After that the results are added together to obtain the total radiated fields by a TD coil.

The aforementioned numerical method is rather complicated and cannot provide any insight into the radiation pattern of a TD coil. Thus, a formula in similar format as (1),which can express the radiated fields in one coordination, is highly desired for the TD coil. In this paper, (1) is transformed into vector spherical wave functions[9]. Then, by using rotation theorem, the radiated fields from C_x and C_y are transferred to the coordination of C_z. In the end, we can obtain a set of much simpler formulas. Specifically, in vector spherical wave format, (1) can be expressed as

$$\mathbf{H} = -\frac{jk^3 a^2 N I_z}{4}\mathbf{N}^3_{01}(kr, \theta, \phi), \tag{2}$$

where $\mathbf{N}^3_{01}(kr, \theta, \phi)$ is the vector spherical wave function and detailed expression is provided in Appendix I. We provide the proof of that (2) is equivalent to (1) in Appendix II.

According to the rotation theorem [10], the vector spherical

wave function can be expressed as

$$\mathbf{N}^3_{01}(kr',\theta',\phi') = \sum_{t=-1}^{1} D_{01t}(\alpha,\beta,\gamma)\mathbf{N}^3_{t1}(kr,\theta,\phi), \tag{3}$$

where $D_{01t}(\alpha,\beta,\gamma)$ is the rotation coefficient and (α,β,γ) are the three Euler angles describing a rotation from primed coordination to unprimed coordination. The detailed expression for $D_{01t}(\alpha,\beta,\gamma)$ is provided in Appendix III.

After rotating the radiated spherical wave generated by UD coil C_x and C_y to the coordination of C_z, we can obtain

$$\begin{aligned}\mathbf{H}^d_t = -\frac{jk^3a^2N}{4}\Big\{&I_z\mathbf{N}^3_{01}(kr,\theta,\phi)\\ &+I_x\left[\mathbf{N}^3_{-11}(kr,\theta,\phi)-\frac{1}{2}\mathbf{N}^3_{11}(kr,\theta,\phi)\right]\\ &+I_y\left[j\mathbf{N}^3_{-11}(kr,\theta,\phi)+\frac{j}{2}\mathbf{N}^3_{11}(kr,\theta,\phi)\right]\Big\}.\end{aligned} \tag{4}$$

Expanding the vector spherical wave functions, we can find the radiated magnetic fields by the TD coil in similar format as (1), which are

$$\begin{aligned}\mathbf{h}^d_r = &\frac{jka^2N}{2r^2}\left(I_z\cos\theta + I_y\sin\phi\sin\theta + I_x\cos\phi\sin\theta\right)\\ &\cdot\left[1+\frac{1}{jkr}\right]\cdot e^{-jkr}\hat{r},\end{aligned} \tag{5a}$$

$$\begin{aligned}\mathbf{h}^d_\theta = &-\frac{k^2a^2N}{4r}\left(I_z\sin\theta + I_y\sin\phi\cos\theta + I_x\cos\phi\cos\theta\right)\\ &\cdot\left[1+\frac{1}{jkr}-\frac{1}{(kr)^2}\right]\cdot e^{-jkr}\hat{\theta},\end{aligned} \tag{5b}$$

$$\mathbf{h}^d_\phi = \frac{k^2a^2N}{4r}\left(I_y\cos\phi - I_x\sin\phi\right)\cdot\left[1+\frac{1}{jkr}-\frac{1}{(kr)^2}\right]\cdot e^{-jkr}\hat{\phi}, \tag{5c}$$

where superscript d denotes the direct path.

Comparing (5) with (1), we can find that the radiated fields from a single UD coil is highly directional, while the TD coil is almost an isotropic radiator. In the near region, magnetic field in $\hat{r}$ direction is dominant. In (1), $\mathbf{h}_r$ only has a $\cos\theta$ which results in a null in magnitude when θ is $\pi/2$. While, in (5), since $\mathbf{h}^d_r$ has both $\sin\theta$ and $\cos\theta$, it has less fluctuation in magnitude when θ is in [0,π]. Similarly, in the far field region, where the magnetic field in $\hat{\theta}$ direction is dominant, $\mathbf{h}^d_\theta$ is more stable than $\mathbf{h}_\theta$ due to the same reason as that in the near region. Therefore, the magnetic field radiated from the TD coil is less directional than that from the UD coil.

C. Underwater Magnetic Field of Tri-directional Coil Antenna

To comprehensively model the underwater MI channel shown in Fig. 1, three field components need to be considered: the direct path, the path reflected on the water surface, and the lateral wave path.

1) Lateral Waves Generated by TD Coil: In the shadow waters, the effects of lateral wave path can be dominant in MI communications. Consider a coil submerged underwater, it can produce a sheet of current on the air-water interface. The current can work as an antenna that radiates EM waves into air. The propagating waves are diffracted into water again and partially reach the receiver in the end. Thus, the lateral waves experience much weaker dissipation since it propagates in lossless air medium.

TABLE I. Simulation Parameters

μ_0	$4\pi\times10^{-7}$ H/m	μ_2	μ_0	μ_1	μ_0	d	0.3 m
ϵ_0	8.854×10^{-12}F/m	ϵ_1	ϵ_0	ϵ_2	$81\epsilon_0$	σ	1 S/m
ω	$2\pi\times10^7$ rad/s	I_0	1 A	N	10	a	0.05 m

We adopt the methods of lateral wave analysis provided in [6] to analyze the MI channel in shadow waters. For a vertical magnetic UD coil C_z, the lateral wave can be written as

$$\begin{cases}\mathbf{h}^{lz}_\rho &= -\frac{jk_1^2a^2NI_z}{2k_2}e^{-jk_2(-z+2d)-jk_1\rho}f(\rho)\hat{\rho},\\ \mathbf{h}^{lz}_z &= -\frac{jk_1^3a^2NI_z}{2k_2^2}e^{-jk_2(-z+2d)-jk_1\rho}g(\rho)\hat{z},\end{cases} \tag{6}$$

where $f(\rho) = -\frac{jk_1}{\rho}-\frac{1}{\rho^2}-\frac{k_1^3}{k_2}\left(-\frac{\pi}{k_1\rho}\right)^{1/2}e^{jp}\mathcal{F}(-p)$, $g(\rho) = f(\rho) - \frac{j}{k_1\rho^3}$, $p = \frac{k_1^3\rho}{2k_2^2}$, and $\mathcal{F}(p) = \frac{1}{2}(1+j) - C_2(p) - jS_2(p)$,where $C_2(p)$ and $S_2(p)$ are Fresnel integral.

The lateral wave radiated by the two horizonal magnetic UD coil C_x and C_y can be put together which are

$$\begin{cases}\mathbf{h}^{ly}_\rho + \mathbf{h}^{lx}_\rho &= \frac{-jNa^2k_1}{2}e^{-jk_2(-z+2d)-jk_1\rho}g(\rho)(I_x\cos\phi - I_y\sin\phi)\hat{\rho},\\ \mathbf{h}^{ly}_z + \mathbf{h}^{lx}_z &= \frac{-jNa^2k_1^2}{2k_2}e^{-jk_2(-z+2d)-jk_1\rho}f(\rho)(I_x\cos\phi - I_y\sin\phi)\hat{z},\\ \mathbf{h}^{ly}_\phi + \mathbf{h}^{lx}_\phi &= \frac{-Na^2}{\rho}e^{-jk_2(-z+2d)-jk_1\rho}f(\rho)(I_x\sin\phi + I_y\cos\phi)\hat{\phi}.\end{cases} \tag{7}$$

It should be noted that the electric field is not formulated in this paper since the MI communication only utilizes the magnetic field.

2) Reflected Filed on the Water Surface: The reflected magnetic field can be derived by using image theory. As shown in Fig. 3, at point o' $(0,0,2d)$, there is an image of the transmitter and we can derive the magnetic dipole moment for the image. Since the water has much larger relative permittivity (81) and conductivity (1 S/m) than air, the reflection coefficient is almost -1. Therefore, we consider the source and the image have the same dipole moment and radiation pattern, except that the vertical dipole moment has opposite direction to its image. In the following discussion, we use a superscript r to denote the reflected magnetic field, i.e., $\mathbf{h}^r_{r,\theta,\phi}$.

We can obtain the radiated field from the image by substituting (r,θ,ϕ) in (5) with (r',θ',ϕ'). The expressions for (r',θ',ϕ') in the coordination provided in Fig. 3 are $r' = \sqrt{(r\sin\theta)^2+[2d+r\cos(\pi-\theta)]^2}$, $\theta' = \frac{\pi}{2}+\arccos(r\sin\theta/r')$ and $\phi' = \phi$.

3) Overall Underwater Magnetic Field: Finally, by combining the direct path, reflected path and lateral wave, the underwater magnetic field at any point can be derived:

$$\begin{cases}\mathbf{h}^o_\rho = (h^d_r\sin\theta + h^d_\theta\cos\theta + h^r_r\sin\theta' + h^r_\theta\cos\theta' + h^{lz}_\rho + h^{ly}_\rho + h^{lx}_\rho)\hat{\rho},\\ \mathbf{h}^o_z = (h^d_r\cos\theta - h^d_\theta\sin\theta + h^r_r\cos\theta' - h^r_\theta\sin\theta' + h^{lz}_z + h^{ly}_z + h^{lz}_z)\hat{z},\\ \mathbf{h}^o_\phi = (h^d_\phi + h^r_\phi + h^{ly}_\phi + h^{lx}_\phi)\hat{\phi},\\ \mathbf{H}^o = \mathbf{h}^o_\rho + \mathbf{h}^o_z + \mathbf{h}^o_\phi.\end{cases} \tag{8}$$

D. FEM Simulation and Numerical Analysis

In this subsection, we use FEM based software Comsol Multiphysics to simulate the magnetic field intensity in various underwater environments. The effects of antenna's depth, orientation, and water's conductivity are evaluated. The simulation model in Comsol AC/DC module is presented in Fig. 5. The infinite element is utilized to extend the simulation environment to infinity. The TD coil is submerged at depth 30 cm. The coil size and frequency are the same as default settings given at the beginning of Section II. We measure the magnetic

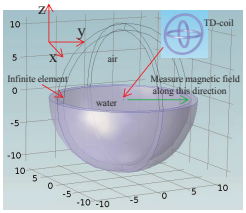

Fig. 5. 3D simulation model.(unit: m)

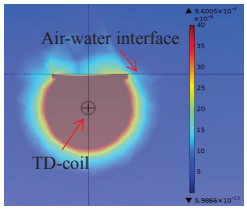

Fig. 6. Visualized magnetic field (Unit: A/m).

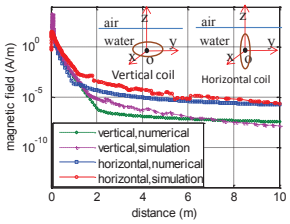

Fig. 7. Orientation effect on radiated magnetic field with single UD coil. (σ = 1 S/m)

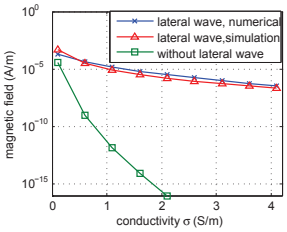

Fig. 8. TD coil: conductivity effect on magnetic field.

field (unit: H/A) with different depth along y-axis direction. The simulation and numerical parameters are provided in Table I. According to the comparisons given in Fig. 7 and Fig. 9, the theoretical curves match the simulation very well, which validate the developed field model.

In Fig. 6, we show the radiated magnetic field from a TD coil. As predicted, on the boundary, the magnetic field is reflected back and very limited portion transmitted into air. Moreover, the radiated magnetic field intensity is not directional. In other words, the TD coil is almost an isotropic radiator and the wireless coverage is omnidirectional.

In Fig. 7, we compare the radiated magnetic field intensity from a vertical UD coil and a horizontal UD coil. We observe that the magnetic field intensity radiated by a vertical coil is almost 2 orders smaller than that radiated by a horizontal coil. The induced current on the surface by a vertical coil is much smaller than a horizontal coil, which results in the weaker magnetic field. On the contrary, the field generated by the TD coil is orientation-independent and achieves the maximum magnetic field at any directions.

In Fig. 8, the effect of water conductivity is presented. The magnetic field is measured at 4 m from transmitting TD coil and the conductivity ranges from 0.1 S/m to 4 S/m. If we consider there is no boundary or water surface, i.e., no lateral waves and reflected path, the magnetic field decreases exponentially. The EM field almost cannot propagate at all in water with high conductivity. However, in the shallow water with air-water interface, both the simulation and numerical results show that the magnetic field decreases much slower as the conductivity increases.

In Fig. 9, the effect of depth from the water surface is discussed. The depth of the transmitter TD coil is kept at 30 cm while the depth of the receiver is gradually increased from 10 cm to 70 cm along y-axis direction. Since the lateral wave is a function of $e^{-jk_2(-z+2d)}$, a larger depth d would cause significant loss due to the complex k_2. Thus, the lateral wave can only take effect near the surface of the water. If we further increase the depth, the contributions from the lateral waves may disappear.

III. Underwater Channel Model

Based on the field analysis, the MI underwater channel is developed in this section. In this section, the transmitter's three

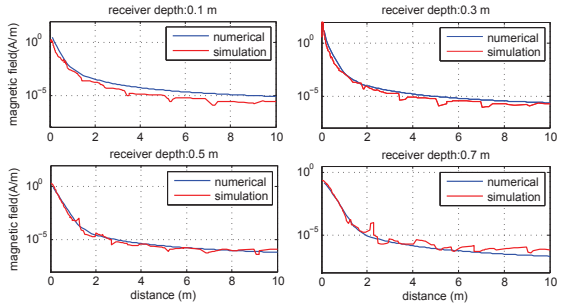

Fig. 9. TD coil magnetic field vs depth.(σ = 1 S/m)

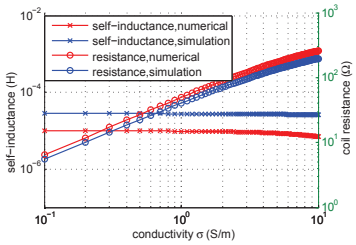

Fig. 10. A UD coil's self-inductance and resistance vs conductivity.

UD coils are labeled with C_1, C_2, and C_3. While the receiver's three UD coils are labeled with C_4, C_5, and C_6.

A. Mutual Inductance

Since the communication range and wavelength are much larger than coil radius, we can safely assume that the magnetic fields through a receiving coil has a constant value. Referring to (8), we denote the magnetic field at the center of a receiving TD coil as $\mathbf{H}^o$. We let C_1 transmit while turning off C_2 and C_3. Then the mutual inductances between C_1 and any of the three UD coils at the receiver are given by

$$M_{1\to v} = \frac{\Phi_{1\to v}}{I_1} = \frac{N\pi a^2 \mu_2 \mathbf{H}_1^o \cdot \mathbf{n}_v}{I_1}, \tag{9}$$

where v =4, 5, or 6, $\mathbf{n}_v$ is the orientation of receiving UD coil C_v, and $\Phi_{1\to v}$ is the magnetic flux through the receiving UD coil C_v generated by C_1. Through the same procedure, the mutual inductances $M_{2\to v}$ and $M_{3\to v}$ can be derived.

Since the induced current at the receiver can generate new magnetic field, the reflected field from the receiver also needs to be considered, which depends on the backward mutual inductance from the receiver to the transmitter. Usually, the mutual inductance is reciprocal, i.e. $M_{1\to v} = M_{v\to 1}$. However, due to the reflected field and lateral waves, if the depth of the transmitter and receiver are different, the mutual inductances of the two directions can also be different. In order to find the mutual inductance between $M_{v\to 1}$, we follow the same strategy as (9).

B. Self-inductance

When a coil is placed above or inside lossy media, there is an additional resistance caused by the eddy current. This additional resistance can be utilized to detect the eddy current in conductors. In this paper, the self-inductance is considered as a complex number, i.e. $L = L_r - jL_i$, where L_r is the real part, L_i is the imaginary part, and both of them are real positive number. Since the impedance of an inductor is $Z_L = j\omega L = j\omega L_r + \omega L_i$, the imaginary part is actually the

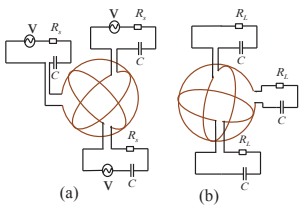

Fig. 11. (a)TD coil transmitter; (b) TD coil receiver.

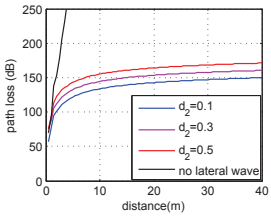

Fig. 12. Effect of receiver's depth on path loss. (d_2's unit:meter, σ = 1 S/m)

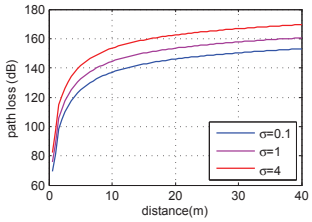

Fig. 13. Effect of conductivity on path loss. (receiver's depth is 0.3 m)

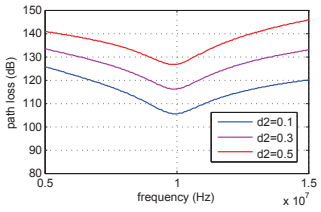

Fig. 14. Frequency response.(d2 is receiver's depth,unit: m; σ = 1 S/m)

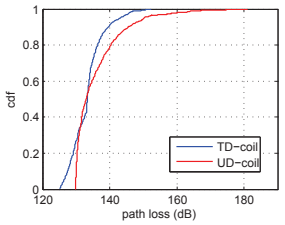

Fig. 15. Orientation effect on path loss.(σ = 1 S/m,receiver's depth is 0.3 m)

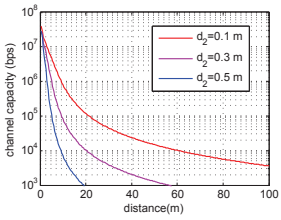

Fig. 16. Channel capacity. (transmitter's depth is 0.3 m, receiver's depth are 0.1 m, 0.3 m, and 0.5 m)

additional resistance. In this paper, the UD coil resistance is written as $R_c^{total} = R_c + \omega L_i$, where R_c is the coil's intrinsic resistance.

The reflected field and lateral wave does not affect the self-inductance. We only consider the magnetic flux generated by the direct field. Thus, the self-inductance of a coil can be expressed as

$$L = \frac{\Phi_0}{I_0} = \frac{N^2 \pi a \mu_2}{2} \left[\cos(k_{2r}a) - j\sin(k_{2r}a)\right] e^{-k_{2i}a}, \qquad (10)$$

where Φ_0 is the magnetic flux through the coil, I_0 is coil's current, k_{2r} and k_{2i} are the real and imaginary part of k_2 respectively, which can be expressed as

$$k_{2r} = 0.707\omega\sqrt{\mu_2\epsilon_2}\left\{[1 + (\sigma/\omega\epsilon_2)^2]^{\frac{1}{2}} + 1\right\}^{\frac{1}{2}},$$
$$k_{2i} = 0.707\omega\sqrt{\mu_2\epsilon_2}\left\{[1 + (\sigma/\omega\epsilon_2)^2]^{\frac{1}{2}} - 1\right\}^{\frac{1}{2}}. \qquad (11)$$

In Fig. 10, the self-inductance and resistance of underwater MI transceiver is plotted as a function of the water conductivity through the FEM simulation and numerical calculation. The coil has the same parameter as in Table I and coil's wire is AWG 26. When conductivity is 0.1 S/m, coil's resistance is less than 10 Ω, while the conductivity is 4 S/m, the resistance is more than 100 Ω. Meanwhile, the real self-inductance is slightly decreased.

C. Equivalent Circuit and Path Loss

Based on the mutual inductance and self-inductance for the UD coils, the equivalent circuit model for TD coil transmitter and TD coil receiver are demonstrated in Fig. 11. The three transmitting UD coil have the same V. R_s is the source resistance and R_L is the load resistance, which both are set as 50 Ω. C is a capacitor which is utilized to match with the coil's real self-inductance and $C = 1/\omega_0^2 L_r$, where ω_0 is the resonant frequency. Once the input voltage V of the transmitter is given, the current in each UD coil can be derived by using Kirchhoff's voltage law, i.e. $\mathbf{ZI} = \mathbf{V}$, where $\mathbf{Z}$ is a 6 by 6 impedance matrix, $\mathbf{I}^T(\cdot) = [I_1, I_2, I_3, I_4, I_5, I_6]$, and $\mathbf{V}^T(\cdot) = [V, V, V, 0, 0, 0]$. If the column w and row v are equal, $\mathbf{Z}(w, v) = Z_c$. For a transmitting UD coil, $Z_c = R_c + R_s + j\omega L + 1/j\omega C$ and for a receiving UD coil, $Z_c = R_c + R_L + j\omega L + 1/j\omega C$. While, if $0 < |w - v| < 3$, $\mathbf{Z}(w, v) = 0$. For other elements in $\mathbf{Z}$, $\mathbf{Z}(w, v) = j\omega M_{w\to v}$. Then, the currents can be solved by $\mathbf{I}(\cdot) = \mathbf{Z}^{-1}\mathbf{V}(\cdot)$.

Finally, the path loss can be expressed by

$$\mathcal{L}(\omega) = -10 \times \log \frac{P_r}{P_t} = -10 \times \log \frac{\sum_{v=4}^{6} |\mathbf{I}(v)|^2 R_L}{\sum_{v=1}^{3} \Re[V\mathbf{I}(v)]}. \qquad (12)$$

Similar to [11], the other important channel parameters, including the bandwidth and channel capacity, can be derived using the path loss model.

IV. Channel Characteristics and Numerical Analysis

In this section, we numerically evaluate the channel characteristics of underwater MI communication using TD coil. The effects of water conductivity, antenna orientation, and antenna depth on channel path loss are evaluated and the channel frequency response, and channel capacity are discussed. In the following analysis, the parameters are kept the same as the simulation in Section II.

First, referring to Fig. 12, we keep the transmitter at depth 0.3 m and gradually increase the depth of the receiver from 0.1 m to 0.5 m. In the vicinity of the TD coil, i.e. less than 1 m, the path loss increases very fast since the direct path and reflected path are dominant. As the distance becomes larger, the lateral wave begins to take strong effect. Since it suffers from lower loss in the air medium, it decreases much slower. However, if we increase the depth, the lateral wave experiences strong absorbtion when it propagates downward to the receiver. Therefore, the lateral wave only take effects in the shallow water. In order to show the lateral wave's significant contribution, we compare the results with the case where antenna is in infinite water medium, i.e. no lateral wave. As shown in the figure, the path loss increases dramatically.

Fig. 13 shows the effect of water's conductivity on path loss. The same as the magnetic field in Fig. 8, the higher conductivity would cause higher loss. Fig. 14 shows the frequency response of the underwater channel for TD coil. Since the coil are tuned to be resonant at 10 MHz, the coil impedance would be greatly increased by further increasing or decreasing the frequency, which in turn increases the path loss.

The coil orientation effect is shown in Fig. 15, where the TD coil transceivers and single UD coil transceivers are compared. We fix the orientation of the transmitter for both UD coil (horizontal) and TD coil (orientation is the same as Fig. 2(d)) and randomly generate the orientation of the UD coil receiver and TD coil receiver. For a UD coil, we randomly generate a unit vector $[\sin\theta\cos\phi, \sin\theta\sin\phi, \cos\theta]$ in 3D space to denote its orientation, where θ and ϕ are uniformly distributed in $[0,\pi]$ and $[0,2\pi]$, respectively. While for a TD

coil, we use the same way to randomly generated the first unit vector. Then, as shown in Fig. 2(b), the second vector $\mathbf{q}$ is uniformly distributed in [0,2π] on the first coil's plane. After that, the third unit vector is determined by the first two vectors. The cumulative distribution function (cdf) of the path loss for UD and TD coil transceivers are evaluated in Fig. 15. The variation of the UD coil's path loss is around 50 dB while TD coil's path loss is around 25 dB. Also, we notice that, a UD coil may obtain a much higher path loss than TD coil, i.e. around 180 dB, which means the performance of UD coil is hard to predict and we have to use high transmission power to always fulfill the basic requirement for received power. Thus, TD coil is more reliable than UD coil.

The Shannon channel capacity of the underwater MI communication is plotted in Fig. 16. The transmitter's depth is 0.3 m and receiver's depth is changing from 0.1 m to 0.5 m. The 3 dB bandwidth is measured from the frequency response and the transmission power is set as 10 dBm. As reported in [12], the measured underwater noise level for MI communication is -120 dBm. From Fig. 16 we find that when receiver is submerged at depth 0.5 m, the communication range can be as far as 20 m with 1 kbps data rate in the conductive salty water. The communication range to coil radius ratio ($\frac{r}{a}$) is 400 with conductivity 1 S/m. Therefore, in shallow water, the lateral wave can greatly increase the communication range. Also, we observe that the depth has great effect on channel capacity. With 0.1 m depth, the range is more than 100 m.

V. Conclusion

In underwater communications, the MI technique shows unique advantages in reliability and low-latency over conventional technologies that are based on optical waves, acoustic waves, and EM waves. In this paper, an accurate and comprehensive channel model is developed for underwater MI system. Different from existing MI underwater channel models, the effect of lateral waves as well as the reflected waves in shallow water region is quantitatively characterized. Moreover, the Tri-directional coil (TD coil) is utilized and modeled to establish an omnidirectional and reliable underwater MI links. Through the modeling and analysis, we observe that the communication range of a MI system using small-size antennas (5 cm in radius) can be as long as 20 m in underwater environment with high water conductivity. Thanks to the omnidirectional coverage brought by the TD coil antennas, the established MI link is also robust to the dynamic rotations of the underwater devices. The developed channel model is verified by FEM simulations.

A. Vector Spherical Wave Function

The VSWFs utilized in this paper follow [9] which can be given by

$$\mathbf{M}^q_{mn}(kr,\theta,\phi) = b^q_n(kr)\times\left[\hat{\theta}\frac{jm}{\sin\theta}P^m_n(\cos\theta) - \hat{\phi}\frac{d}{d\theta}P^m_n(\cos\theta)\right]e^{jm\phi}; \tag{13a}$$

$$\mathbf{N}^q_{mn}(kr,\theta,\phi) = \hat{r}\frac{n(n+1)b^q_n(kr)}{kr}P^m_n(\cos\theta)e^{jm\phi} + \frac{b^q_n(kr)+krb^{q\prime}_n(kr)}{kr} \times\left[\hat{\theta}\frac{d}{d\theta}P^m_n(\cos\theta) + \hat{\phi}\frac{jm}{\sin\theta}P^m_n(\cos\theta)\right]e^{jm\phi}. \tag{13b}$$

where $P^m_n(\cos\theta)$ is the associated legendre polynomials, $b^q_n(kr)$ is the spherical Bessel functions. The value of q can be 1,2,3, and the corresponding $b^q_n(kr)$ are the first kind of spherical Bessel function $j_n(kr)$, spherical Neumman function $y_n(kr)$, and spherical Hankel function of the second kind $h^2_n(kr)$, respectively. Since the infinitesimal magnetic dipole only radiates TE_{10}, so here n=1 and m=0.

B. Proof of the Equalization of (1) and (2)

Note that $e^{-jkr} = \cos(kr) - j\sin(kr)$. Then we can expand (1) and obtain the following equations. $\frac{1}{r^2}[1+\frac{1}{jkr}]e^{-jkr} = -\frac{k}{r}h^2_1(kr)$, and $\frac{1}{r}[1+\frac{1}{jkr}-\frac{1}{(kr)^2}]e^{-jkr} = -\frac{j}{r}[h^2_1(kr)+krh^{2\prime}_1(kr)]$, where $h^2_1(kr)$ is the second kind of spherical Hankel function of order 1. In addition, the associated legendre polynomial $P^0_1(\cos\theta) = \cos\theta$. Putting together, we can obtain

$$\begin{aligned}\mathbf{H}_z =& \mathbf{h}_r + \mathbf{h}_\theta + \mathbf{h}_\phi = -\frac{jk^3a^2I_z}{4}\left\{\hat{r}\frac{2h^2_1(kr)}{kr}P^0_1(\cos\theta)e^{j\phi\cdot0}\right.\\ &\left.+\frac{h^2_1(kr)+krh^{2\prime}_1(kr)}{kr}[\hat{\theta}\frac{d}{d\theta}P^0_1(\cos\theta)+\hat{\phi}\cdot0]\cdot e^{j\phi\cdot0}\right\}\\ =& -\frac{jk^3a^2I_z}{4}\mathbf{N}^3_{01}(kr,\theta,\phi).\end{aligned} \tag{14}$$

C. Rotation Theorem

The rotation theorem for vector spherical wave functions can rotate the spherical waves between two coordinations which have the same origin but different directions. According to [10], $D_{01t}(\alpha,\beta,\gamma)$ in (3) can be expressed as

$$D_{01t}(\alpha,\beta,\gamma) = e^{j\gamma\cdot0}P^{-t}_1(\cos\beta)e^{jt\alpha} = P^{-t}_1(\cos\beta)e^{jt\alpha}, \tag{15}$$

where $P^t_1(\cos\beta)$ is the associated legendre polynomial.

References

[1] I. Akyildiz, D. Pompili, and T. Melodia, "Underwater acoustic sensor networks: Research challenges," *Elsevier's Journal of Ad Hoc Networks*, vol. 3, no. 3, pp. 257–279, 2005.

[2] Z. Sun and I. F. Akyildiz, "Magnetic induction communications for wireless underground sensor networks," *IEEE Transactions on Antenna and Propagation*, vol. 58, no. 7, pp. 2426–2435, July 2010.

[3] A. Al-Shamma'a, A. Shaw, and S. Saman, "Propagation of electromagnetic waves at mhz frequencies through seawater," *Antennas and Propagation, IEEE Transactions on*, vol. 52, no. 11, pp. 2843–2849, Nov 2004.

[4] M. C. Domingo, "Magnetic induction for underwater wireless communication networks," *IEEE Transactions on Antennas and Propagation*, vol. 60, no. 6, pp. 2929–2939, 2012.

[5] B. Gulbahar and O. B. Akan, "A communicatiion theoretical modeling and analysis of underwater magneto-inductive wireless channels," *IEEE Transactions on Wirelss Communications*, vol. 11, no. 9, pp. 3326–3334, 2012.

[6] R. King, "Electromagnetic surface waves: New formulas and applications," *Antennas and Propagation, IEEE Transactions on*, vol. 33, no. 11, pp. 1204–1212, Nov 1985.

[7] S. Stein, "Addition theorems for spherical wave functions," *Quart. Appl. Math.*, vol. 19, 1961.

[8] C. A. Balanis, *Antenna Theory*. John Wiley Publishing Company, 2005.

[9] L. Tsang, J. Kong, and K. Ding, *Scattering of Electromagnetic Waves, Theories and Applications*, ser. A Wiley interscience publication. Wiley, 2000.

[10] D. W. Mackowski, "Analysis of radiative scattering for multiple sphere configurations," *Proceedings of the Royal Society of London. Series A: Mathematical and Physical Sciences*, vol. 433, no. 1889, pp. 599–614, 1991.

[11] H. Guo and Z. Sun, "Channel and energy modeling for self-contained wireless sensor networks in oil reservoirs," *IEEE Transactions on Wireless Communications*, vol. 13, no. 4, pp. 2258–2269, April 2014.

[12] C. Uribe and W. Grote, "Radio communication model for underwater wsn," in *New Technologies, Mobility and Security (NTMS), 2009 3rd International Conference on*, Dec 2009, pp. 1–5.